EUROPEAN ORGANIZATION FOR NUCLEAR RESEARCH

CERN-PPE/97-XXX
July 3, 1997

Measurement of the $\eta^{'}(958)$ formation in Two-Photon Collisions at LEP

The L3 Collaboration

Abstract

The formation of the $\eta^{'}$ in the reaction $e^+e^- \to e^+e^-\eta^{'} \to e^+e^-\pi^+\pi^-\gamma$ has been measured by the L3 detector at a centre-of-mass energy of 91 GeV. The radiative width of the $\eta^{'}$ for quasi-real photons has been found to be $\Gamma_{\gamma\gamma} = 4.17 \pm 0.10$ (stat.) $\pm$ 0.27 (sys.) keV. The Q^2 dependence of the $\eta^{'}$ formation cross section has been studied for Q^2 less than 10 GeV^2. The $\eta^{'}$ electromagnetic transition form factor has been measured, it can be parametrised by a pole form $\Lambda = 0.903 \pm 0.046$ (stat.) $\pm$ 0.034 (sys.) GeV. The data are also consistent with recent non-perturbative QCD calculations.

Submitted to *Phys. Lett.*

1 Introduction and formalism

The formation of the $\eta^{'}(958)$ is studied in the two-photon reaction $\mathrm{e^+e^-} \to \mathrm{e^+e^-}\eta^{'}$, $\eta^{'} \to \pi^+\pi^-\gamma$, by using data collected with the L3 detector at LEP at the centre-of-mass energies $\sqrt{s} \simeq 91$ GeV. The four-momenta transfer of the scattered electrons, q^2 and k^2, is often so small that the electrons go undetected along the beam. The photon with highest virtuality defines the variable Q^2 = -q^2. If one of the electrons is detected, the event is said to be *tagged*. The strength of the coupling of a meson to two photons, $\Gamma_{\gamma\gamma}$, and the Q^2 dependence of the formation cross section give information on the quark content and on the quark dynamics of the bound state.

The cross section for the formation of a resonance R is given by:

$$\sigma(\mathrm{e^+e^-} \to \mathrm{e^+e^-R}) = \int d^5\mathcal{L}_{\gamma\gamma}(\alpha_i) \cdot \sigma(W_{\gamma\gamma}, q^2, k^2) \tag{1}$$

where $d^5\mathcal{L}_{\gamma\gamma}$ is the differential luminosity function giving the flux of virtual photons and $\alpha_i (i = 1, ..., 5)$ are the variables describing the scattered electron and positron. The Q^2 dependence of the cross section is expressed by the meson electromagnetic form factor F

$$\sigma(W_{\gamma\gamma}, q^2, k^2) = \frac{\pi}{4}\sqrt{X} \cdot F^2(q^2, k^2) \cdot \sigma(W_{\gamma\gamma}, 0, 0) \tag{2}$$

where X is the Møller flux factor $[(q \cdot k)^2 - q^2k^2]$. The form factor F is usually parametrised with a pole form,

$$\frac{F^2(q^2, k^2)}{F^2(0,0)} = [\frac{1}{1 - q^2/\Lambda^2}]^2 \cdot [\frac{1}{1 - k^2/\Lambda^2}]^2 \quad \text{where} \quad F^2(0,0) = \frac{64\pi}{m_R^3}\Gamma_{\gamma\gamma} \tag{3}$$

The parameter Λ is related to the size of the meson [1] and must be described by any model of $q\bar{q}$ binding.

Combining Eq. 1-3 leads to the proportionality relation

$$\sigma(\mathrm{e^+e^-} \to \mathrm{e^+e^-R}) = \mathcal{K} \cdot \Gamma_{\gamma\gamma} \tag{4}$$

which allows the determination of the two-photon partial width of the resonance from the measurement of its production cross section.

The decay rate of $\eta^{'} \to \rho\gamma$ in the two-photon centre-of-mass frame is

$$d\Gamma_{\eta' \to \rho\gamma} = \frac{1}{32\pi^2} |\mathcal{M}|^2 \frac{p_\gamma}{m_{\eta'}^2} d\Omega \tag{5}$$

Since the $\eta^{'}$ is a spin 0 particle, the transition $0^- \to 1^- + 1^-$ requires that in the ρ rest frame the decay amplitude is

$$\mathcal{M} = BW(\rho) \cdot \sqrt{2} m_{12} \mathrm{p}_1^* \mathrm{p}_\gamma^* \sin\theta_1^* \tag{6}$$

where m_{12} is the mass of the $\pi^+\pi^-$ system, p_γ^* is the photon momentum, p_1^* is the π^+ momentum and θ_1^* is the angle between the π^+ and the photon direction. Recently it has been discussed [2, 3] that a pure ρ Breit-Wigner term is not sufficient to describe the data. A non-resonant contribution in the $\eta' \to \rho\gamma$ decay associated with a possible box anomaly contribution has been included [2, 3] by adding a second term to the ρ Breit-Wigner:

$$BW(\rho) = \frac{1}{(m_{12}^2 - m_\rho^2) - im_{12}\Gamma_\rho} + \frac{\xi}{m_{\eta'}} exp(i\phi) \tag{7}$$

where ξ is the relative amplitude with phase angle ϕ. For the ρ mass dependent width Γ_ρ, the formula of Ref. [4] is used in the present analysis :

$$\Gamma_\rho = \Gamma_0 \left(\frac{p_1^*}{p_0}\right)^3 \frac{m_\rho}{m_{12}} \tag{8}$$

where $p_0 = \sqrt{m_\rho^2 - 4m_{\pi^+}^2}/2$ and $\Gamma_0 = 151.2$ MeV is the nominal width of the ρ [5].

The EGPC Monte Carlo [6] is used to generate the events. The events $e^+e^- \to e^+e^- X$ are generated according to the $\mathcal{L}_{\gamma\gamma}$ luminosity function of Budnev et al [7]. The Breit-Wigner shape, the form factor and the decay of the system X are then implemented as described by Eq. 2-6. The resonance parameters are taken from Ref. [5], except for the $\Gamma_{\gamma\gamma}(\eta')$ width which is fixed to 1 keV. The Monte Carlo events were simulated in the L3 detector using GEANT [8] and GEISHA [9] programs and passed through the same reconstruction program as the real data.

2 Data analysis

2.1 Event selection

The L3 detector [10] has the capability to measure charged particles and photons of low momentum. A trigger, which requires at least two charged particles with $p_t > 150$ MeV back-to-back in the transverse plane within 41°, allows an efficient acquisition of two-photon events. For tagged events the trigger demands at least 30 GeV deposited in the small angle electromagnetic calorimeter in coincidence with at least one track in the central part of the detector.

The candidate $e^+e^- \to e^+e^-\pi^+\pi^-\gamma$ events are selected by requiring:

- *Two oppositely charged tracks.* A track is accepted if it has at least 20 hits out of a maximum of 62 in the central detector and if its transverse momentum p_t is greater than 130 MeV. The total transverse momentum squared of the two charged tracks $|\vec{p_t}(\pi^+\pi^-)|^2$ must be greater than 0.001 GeV^2, to eliminate the lepton channels $e^+e^- \to e^+ e^- l^+l^-$ ($l =$ e, μ).

- *One photon only.* A cluster in the electromagnetic calorimeter is identified as a photon if it has an energy greater than 140 MeV and it is separated by an angle greater than 10° from either track.

- *The angle* of the π^+ in the ρ helicity frame must be such that $|\cos\theta_1^*| < 0.94$. This cut reduces non-resonant exclusive background.

The events are classified in three groups: *a*) the events produced by quasi-real photons ($Q^2 < 0.01$ GeV^2), *b*) the intermediate range ($0.01 \le Q^2 \le 0.9$ GeV^2) where the electron goes undetected and the Q^2 is measured from the transverse momentum of the η' and *c*) the singly tagged events where one electron is detected in the small angle electromagnetic calorimeter ($1.5 \le Q^2 \le 10.0$ GeV^2) .

2.2 Quasi-real photons and $\Gamma_{\gamma\gamma}(\eta^{'})$

For the group *a*) the analysis is limited to photons observed in the polar angle range $45^\circ \leq \theta \leq 135^\circ$ and with $|\overrightarrow{p_t}(\pi^+\pi^-\gamma)|^2 < 0.01$ GeV^2. The $(\pi^+\pi^-\gamma)$ mass spectrum is shown in Fig. 1, 6767 events are selected, where 2786 are in the $\eta^{'}$region $(0.85 \leq M(\pi^+\pi^-\gamma) \leq 1.05$ GeV). The $\eta^{'}$ mass, obtained by a Gaussian fit, is 958 ± 1 MeV with $\sigma = 24 \pm 1$ MeV, a value which agrees well with the $(\pi^+\pi^-\gamma)$ mass resolution as estimated by the Monte Carlo. The enhancement around 1250 MeV is due to the tensor meson, $a_2(1320)$, whose dominant decay mode is: $a_2 \rightarrow \pi^{\mp}\rho^{\pm} \rightarrow \pi^{\pm}\pi^{\mp}\pi^0 \rightarrow \pi^{\pm}\pi^{\mp}\gamma\gamma$. If one of the two photons has low transverse momentum and is undetected, these events can pass the selection cut, creating this enhancement. a_2 events were simulated with the parameters obtained by us and reported in Ref. [11]. The angular distributions were generated according to the measured $J^P(\lambda) = 2^+(2)$ [11]. The simulation of Monte Carlo events takes into account detector and trigger inefficiencies. The reconstruction efficiency for a photon is 97.7 % independent of its energy. The trigger efficiency for group *a*) $\eta^{'}$ events is 48 ± 1 %. In Fig. 2a) the angle distribution of the π^+ in the ρ^0 helicity frame is presented for the events in the $\eta^{'}$ region, it shows the characteristic distribution of Eq. 6.

The two-photon radiative width $\Gamma_{\gamma\gamma}(\eta^{'})$ is determined by fitting the mass spectrum of Fig. 1 with the Monte Carlo distribution for the $\eta^{'}$ and the a_2 and a third order polynomial for the background. The fit minimises a χ^2 function with expected value in bin i of :

$$E_i = [\frac{\Gamma_{\gamma\gamma}(\eta^{'})}{1 \text{ keV}}] \cdot N_i(\eta^{'}) + N_i(a_2) + B_i \tag{9}$$

where N_i are the Monte Carlo expectations for the $\eta^{'}$ and for the a_2. The value of $\Gamma_{\gamma\gamma}(\eta^{'})$ in the generator is fixed to 1 keV. The free parameters are $\Gamma_{\gamma\gamma}(\eta^{'})$ and the coefficients of the polynomial background, B_i. The fitted $\Gamma_{\gamma\gamma}$ width thus obtained is:

$$\Gamma_{\gamma\gamma}(\eta^{'}) = 4.17 \pm 0.10 \text{ (stat.)} \pm 0.27 \text{ (sys.) keV} \qquad \chi^2/\text{D.F.} = 131/121$$

The fit results are superimposed on the data in Fig. 1. The systematic uncertainty for the $\Gamma_{\gamma\gamma}$ measurement is 6.6 % . The main uncertainties come from the branching ratio and the selection cuts : 4.3 % from the branching ratio, 4 % from the cut in the photon energy, 1 % from the cut in $|\overrightarrow{p_t}(\pi^+\pi^-\gamma)|^2$, 2 % for the trigger and 1 % for background subtraction. This result compares well with those of previous experiments [14, 15] in Table 1 and is comparable in precision to the previous world average value, 4.34 ± 0.25 keV [5]. One may note that recent relativistic quark models [12], which successfully predict the two-photon coupling of tensor mesons, fail to reproduce the value of the two-photon widths of pseudoscaler states. The prediction is typically a factor of two below the measurement.

The good resolution of the detector and the high statistics allow an accurate study of the $\eta^{'} \rightarrow \rho\gamma$ decay. In Fig. 2b) the uncorrected $\pi^+\pi^-$ mass spectrum is shown. The ρ line shape given by Eq. 7 and 8 has been studied by constructing 15 Monte Carlo samples with $756 \leq m_\rho \leq 774$ MeV and 12 samples with $130 \leq \Gamma_\rho \leq 160$ MeV. By comparing the data to the Monte Carlo samples, the minimum of the χ^2 ($\chi^2 = 34$ for 32 degree of freedom, C.L.=37 %) is found for the values

$$m_\rho = 766 \pm 2 \text{ MeV} \qquad \Gamma_\rho = 150 \pm 5 \text{ MeV}.$$

These results agree with the world average, $m_\rho = 768.5 \pm 0.6$ MeV and $\Gamma_\rho = 150.7 \pm 1.2$ MeV [5]. With the same method the possibility of a non-resonant $\pi^+\pi^-$ contribution (Eq. 7) has been tested by varying the ξ and ϕ parameters. The best agreement with the data is for $\xi = 0$ and $\phi = 0$. The values obtained by previous analysis $\xi = 2.78$ and $\phi = -1.07$ [2] and $\xi \simeq 0.4$ and $\phi = 3.14$ [3] are disfavoured with a χ^2 of 68 (C.L.$\sim 10^{-2}$ %) and 49 (C.L.=3 %) respectively, for 32 degree of freedom.

2.3 η' transition form factor

For the events of group *b*) in which no tagged electron is found in the forward calorimeters and the total transverse momentum squared of the $(\pi^+\pi^-\gamma)$ system is above 0.01 GeV^2, the Monte Carlo simulation demonstrates that $Q^2 = |\overrightarrow{p_t}(\pi^+\pi^-\gamma)|^2$ within the experimental resolution (Fig. 3). The data are subdivided into three Q^2 intervals (Fig. 4a-c). Although the background is more important in these configurations because there is no efficient cut against events with additional undetected particles, the narrow η' signal is still clearly seen above the background. The number of η' events obtained by a fit of a gaussian, superimposed to a third order polynomial background, is given in Table 2.

The tagged events, group *c*), are selected by requiring a shower in the small angle electromagnetic calorimeter with energy greater than 35 GeV. The total transverse momentum squared of all detected particles must have $|\overrightarrow{p_t}(\mathrm{e}_{tag}\pi^+\pi^-\gamma)|^2 < 0.05$ GeV^2 where e_{tag} is detected electron. The $\pi^+\pi^-\gamma$ mass spectrum of this class of events is shown in Fig. 4d. The η' signal is present with a good resolution ($\sigma = 26$ MeV) over a small background. These tagged events are subdivided into two Q^2 intervals in Table 2.

The cross section is measured in each Q^2 interval as

$$\Delta\sigma = \frac{\Delta N}{\mathcal{L} \times \varepsilon \times Br} \qquad (10)$$

where ΔN is the measured number of η', $\mathcal{L}$ is the total integrated luminosity, ε is the detector acceptance and efficiency and $Br = 0.302$ [5] is the η' branching ratio into the $\pi^+\pi^-\gamma$ channel. The total integrated luminosity is 129 pb^{-1} for untagged events and 100 pb^{-1} for tagged events, since the trigger for tagged events was not operational all the time. The measured cross sections and the average Q^2 are listed in Table 2. The average Q^2 is calculated by taking into account the Q^2 dependence of the spectrum with the Monte Carlo. The systematic uncertainty from the selection is the same in all groups. The additional uncertainty from the background subtraction varies from 6 % to 10 % for different Q^2 intervals.

The decrease of the cross section as function of Q^2 is due to the two-photon luminosity function and to the resonance form factor. The effect of the luminosity function is removed by generating events with a flat form factor ($F(Q^2)/F(0) = 1$). The η' electromagnetic form factor is then given by the ratio :

$$\frac{m^3_{\eta'}}{64\pi} \cdot \frac{F^2(Q^2)}{1\ \mathrm{keV}} = \frac{\sigma_{data}(Q^2)}{\sigma_{flatMC}(Q^2)} \qquad (11)$$

The transition form factor is also corrected for the virtuality of the second photon. The effect is studied by generating events with different input Λ values ($0.77 - 1.01$ GeV) in Eq. 3. The corrected results are given in Table 2 and in Fig. 5. The effect of collinear initial state radiation on the form factor is found to be negligible: it is less than 1 % for group *b*), untagged events, and 3 % for group *c*), tagged events. The five high Q^2 points are fitted with the form factor parametrisation given in Eq. 3. The value at $Q^2 = 0$ is fixed to the measured value of $\Gamma_{\gamma\gamma}$. The fit is illustrated in Fig. 5a; the χ^2 is 2.7 for 4 d.o.f. From the fit a value of $\Lambda = 0.903 \pm$

0.046 (stat.) $\pm$ 0.034 (sys.) GeV is obtained. If the virtuality of the second photon is neglected, the value of Λ would be 11 % lower. We compare our measurement with previous measurement in Table 3. The parameter Λ is related to the interaction size of the $\eta^{'}$: $\langle r^2 \rangle = 6/\Lambda^2$. From these data one obtains $\langle r^2 \rangle = 0.286 \pm 0.016$ fm^2.

For pseudoscalar mesons π^0, η and $\eta^{'}$, there exist several models which describe the transition form factor. The Vector Dominance (VDM) hypothesis identifies Λ with the mass of ρ, ω, ϕ. Its prediction, $\Lambda = 0.83$ GeV [1], is shown in Fig. 5b as a dashed line. Recently many QCD models have been developed to describe the π^0 form factor [16–18]. Ref. [17, 19] also provide predictions for the $\eta^{'}$ form factor, by considering the mixing of the singlet and octet components of the flavour SU(3) pseudoscalar nonet. In the chiral limit of vanishing quark masses the photon-pion transition form factor is fixed by the $\pi^0 \to \gamma\gamma$ decay :

$$F_{\pi\gamma}(q^2 = 0, k^2 = 0) \propto \frac{1}{2\sqrt{2}\pi^2 f_\pi} \qquad \text{where} \qquad f_\pi = 130.7 \text{ MeV} \tag{12}$$

For $k^2 = 0$ and large Q^2 the QCD model of Brodsky and Lepage [13] expresses the form factor in term of the wave function of the quark inside the pion, $\Phi(x)$:

$$F_{\pi\gamma}(Q^2) \propto \frac{2}{\sqrt{3}Q^2} \int_0^1 dx \frac{\Phi(x)}{x(1-x)} \qquad F_{\pi\gamma}(Q^2 \to \infty) \propto \frac{\sqrt{2} f_\pi}{Q^2} \tag{13}$$

where x is the momentum fraction of the quark inside the pion. Brodsky and Lepage interpolate between the $Q^2 = 0$ and $Q^2 \to \infty$ limits with the pole form of Eq. 3 giving a parameter $\Lambda \simeq 0.66$ GeV [1,13]. This prediction is drawn in Fig. 5b as a dashed-dotted line. In their hard scattering approach, Ref. [17] consider also the transverse degree of freedom for the $q\bar{q}$ wave function and include the gluonic corrections in a Sudakov factor. Their calculation is compared to the data in Fig. 5b.

In order to cover the low and moderately high Q^2 region of the photon-meson transition form factor, Ref. [18] introduces the $q\bar{q}$ distribution function G_γ at the $\gamma q\bar{q}$ vertex similar to the pion distribution function G_π describing the $\pi q\bar{q}$ vertex; i.e. the photon is treated much like a vector meson. At large Q^2 the photon wave function also contains the standard QED point-like $q\bar{q}$ coupling. The $O(\alpha_s)$ diagrams of one gluon exchange between two quarks are also taken into account. The transition form factor is thus written by Ref. [18] as a sum of soft and hard components. The parameters of the theory are determined by the data of the elastic pion form factor (G_π) and by the data of the π^o-γ transition form factor (G_γ). With no new parameter and using the value $\sin\beta = 0.61$ for the mixing angle between the $s\bar{s}$ and $(u\bar{u} + d\bar{d})/\sqrt{2}$ components, the same authors calculate the η and $\eta^{'}$ transition form factors [19]. They also explore the possibility that the η and $\eta^{'}$contain an extra glueball component. Their predictions are given in Fig. 5a for a variable admixture of gluon content.

3 Conclusions

A high statistics sample of $e^+e^- \to e^+e^-\eta^{'}$, $\eta^{'} \to \pi^+\pi^-\gamma$ events has been collected with the L3 detector at LEP energies around 91 GeV. From the quasi-real two-photon interaction the $\eta^{'}$ radiative width $\Gamma_{\gamma\gamma}(\eta^{'}) = 4.17 \pm 0.10$ (stat.) $\pm$ 0.27 (sys.) keV is obtained.

The $\eta^{'}$ transition form factor has been measured in the interval $0.01 \leq Q^2 \leq 10.0$ GeV. A fit to the data with a pole parametrisation gives a value $\Lambda = 0.903 \pm 0.046$ (stat.) $\pm$ 0.034 (sys.) GeV. The pole form is a good representation of the data. Recent non-perturbative QCD calculations have also been compared to the data.

Acknowledgements

We wish to thank P. Kroll, V.V. Anisovich and V.A. Nikonov for their help on the theoretic predictions. We express our gratitude to the CERN accelerator divisions for the excellent performance of the LEP machine. We acknowledge with appreciation the effort of all engineers, technicians and support staff who have participated in the construction and maintenance of this experiment.

Collaboration	Decay channel	N_{events}	$\Gamma\gamma\gamma\ (keV)$
L3 (this analysis)	$\pi^+\pi^-\gamma$	2123 ± 53	$4.17 \pm 0.10 \pm 0.21$
PLUTO	$\rho^0\gamma$	243 ± 16	$3.80 \pm 0.26 \pm 0.43$
Crystal Ball	$\gamma\gamma$	136 ± 14	$4.80 \pm 0.50 \pm 0.50$
	$\eta\pi^0\pi^0$	266 ± 17	$4.53 \pm 0.29 \pm 0.49$
MD-1	$\pi^+\pi^-\gamma$	23	$4.60 \pm 1.10 \pm 0.60$
Mark II	$\rho^0\gamma$		$4.57 \pm 0.25 \pm 0.44$
ASP	$\gamma\gamma$	547	$4.94 \pm 0.23 \pm 0.72$
TPC-2γ	$\eta\pi^+\pi^-$	34	$3.80 \pm 0.70 \pm 0.60$
	$\rho^0\gamma$		$4.50 \pm 0.30 \pm 0.70$
CELLO	$\rho^0\gamma$	668 ± 27	$3.62 \pm 0.14 \pm 0.48$
ARGUS	$\rho^0\gamma$	867 ± 30	$3.76 \pm 0.13 \pm 0.47$

Table 1: The two-photon radiative width of the η' with statistical and systematic errors. The values obtained in previous experiments [14, 15] are also refered.

Q^2 interval	$\langle Q^2 \rangle$	η' events	ε	$\Delta\sigma$	$(m^3_{\eta'}/64\pi)F^2(Q^2)$
(GeV^2)	(GeV^2)		(%)	(pb)	(keV)
0.0 – 0.01		2123 ± 53	2.8	$1924 \pm 48 \pm 96$	$4.17 \pm 0.10 \pm 0.27$
0.01 – 0.15	0.06	726 ± 47	3.7	$510 \pm 33 \pm 39$	$3.51 \pm 0.23 \pm 0.27$
0.15 – 0.30	0.23	123 ± 18	2.9	$109 \pm 16 \pm 12$	$2.78 \pm 0.41 \pm 0.30$
0.30 – 0.90	0.53	58 ± 11	1.7	$88 \pm 17 \pm 9$	$1.50 \pm 0.29 \pm 0.15$
1.50 – 2.50	1.90	17 ± 5	5.3	$10.4 \pm 3.3 \pm 1.0$	$0.38 \pm 0.12 \pm 0.04$
2.50 – 10.0	4.14	19 ± 6	10.3	$6.1 \pm 1.8 \pm 0.5$	$0.109 \pm 0.032 \pm 0.01$

Table 2: Number of η' events and cross sections $\Delta\sigma$ as a function of Q^2. The total acceptance and efficiency ε is given. In the last column the electromagnetic transition form factor, corrected for the virtuality of the second photon, is calculated for each $\langle Q^2 \rangle$. The first error is statistical and the second is systematic.

Experiment	Q^2 interval (GeV^2)	Λ GeV
L3 (these data)	0.01-10.	0.903 ± 0.046
TPC/2γ	0.1 - 7.	0.850 ± 0.070
CELLO	0.3 - 20.	0.794 ± 0.044
CLEO	2. - 20.	0.821 ± 0.015
Predictions		
VMD		0.83
Brodsky-Lepage		0.66

Table 3: Measurements of the Λ parameter of the form factor (Eq. 3) compared with previous experiments [15]. The quoted errors are only statistical. The predictions of different models, as presented in Ref. [1] are also given.

References

[1] Ll. Ametler, J. Bijnens, A. Bramon, F. Cornet, Phys. Rev. D 45 (1992) 986 and references therein.

[2] S.I. Bityukov et al., Z. Phys. C 50 (1991) 451.

[3] M. Benayoun et al., Z. Phys. C 58 (1993) 31. PPE /92-156.

[4] J.D. Jackson, Nuovo Cimento 34 (1964) 1644.

[5] Review of Particle Physics, Phys. Rev. D 54 (1996) 192.

[6] EGPC generator used by L3 described in : F.L. Linde, PhD thesis, Rijksuniversiteit te Leiden (1988).

[7] V.M. Budnev et al., Phys. Rep. 15 (1975) 181.

[8] R. Brun et al., GEANT 3.15 preprint CERN DD/EE/84-1 (Revised 1987).

[9] H. Fesefeldt, RWTH Aachen report PITHA 85/2 (1985).

[10] B. Adeva et al., L3 Coll., Nucl. Inst. Meth. A 289 (1990) 35.

[11] L3 Coll., "Resonance Formation in the $\pi^+\pi^-\pi^0$ Final State in Two-Photon Collisions", CERN-PPE/97-68. Phys. Lett. B to be published.

[12] E. Klempt, B.C. Metsch, C.R. Münz, H.R. Petry, Phys. Lett. B 361 (1995) 160.
C.R. Münz, Nucl. Phys. A 609 (1996) 364.

[13] S.J. Brodsky and G. P. Lepage, Phys. Rev. D 24 (1981) 1808.

[14] Antreasian et al, Crystal Ball, Z. Phys. C 54 (1992) 33.
F. Butler et al., Mark II, Phys. Rev. D 42 (1990) 1368.
H.Aihara et al. , TPC/Two-Gamma Coll., Phys. Rev. D 35 (1987) 2650.
H.Aihara et al. , TPC/Two-Gamma Coll., Phys. Rev. D 38 (1988) 1.
Baru S.E. et al., MD-1, Z. Phys. C 48 (1990) 581.
Roe N. et al. ASP, Phys. Rev. D 41 (1990) 17.
Williams D.A. et al., Crystal Ball, Phys. Rev. D 38 (1988) 1365.
H. Albrecht et al., ARGUS Coll., Phys. Lett. B 199 (1987) 457.
Ch. Berger et al., PLUTO Coll., Phys. Lett. 142 (1984) 125.

[15] V. Savinov , CLEO Coll. in Photon '95, pg 203, (X International Workshop on $\gamma\gamma$ collisions) Sheffield(1995).
H.J. Behrend et al , CELLO Coll., Z. Phys. C 49 (1991) 401.
H.Aihara et al. , TPC/Two-Gamma Coll., Phys. Rev. Lett. 64 (1990) 172.

[16] M.R. Frank, K.L. Mitchell, C.D. Roberts and P.C. Tandy, Phys. Lett. B 359 (1995) 17.
D. Kekez and D. Klabucar, Phys. Lett. B 387 (1996) 14.

[17] R. Jacob, P. Kroll and M. Raulfs, J. Phys. G: Nucl. Part. Phys. 22 (1996) 45.

[18] V.V. Anisovich, D.I. Melikhov and V.A. Nikonov, Phys. Rev. D 55 (1997) 2918.

[19] V.V. Anisovich, D.V. Bugg, D.I. Melikhov and V.A. Nikonov, hep-ph/9702383, to be published in Phys. Lett. B.

The L3 Collaboration:

M.Acciarri,[29] O.Adriani,[18] M.Aguilar-Benitez,[28] S.Ahlen,[12] J.Alcaraz,[28] G.Alemanni,[24] J.Allaby,[19] A.Aloisio,[31]
G.Alverson,[13] M.G.Alviggi,[31] G.Ambrosi,[21] H.Anderhub,[51] V.P.Andreev,[7,40] T.Angelescu,[14] F.Anselmo,[10] A.Arefiev,[30]
T.Azemoon,[3] T.Aziz,[11] P.Bagnaia,[39] L.Baksay,[46] S.Banerjee,[11] Sw.Banerjee,[11] K.Banicz,[48] A.Barczyk,[51,49]
R.Barillère,[19] L.Barone,[39] P.Bartalini,[36] A.Baschirotto,[29] M.Basile,[10] R.Battiston,[36] A.Bay,[24] F.Becattini,[18]
U.Becker,[17] F.Behner,[51] J.Berdugo,[28] P.Berges,[17] B.Bertucci,[36] B.L.Betev,[51] S.Bhattacharya,[11] M.Biasini,[19]
A.Biland,[51] G.M.Bilei[36] J.J.Blaising,[4] S.C.Blyth,[37] G.J.Bobbink,[2] R.Bock,[1] A.Böhm,[1] L.Boldizsar,[15] B.Borgia,[39]
D.Bourilkov,[51] M.Bourquin,[21] S.Braccini,[21] J.G.Branson,[42] V.Brigljevic,[51] I.C.Brock,[37] A.Buffini,[18] A.Buijs,[47]
J.D.Burger,[17] W.J.Burger,[21] J.Busenitz,[46] A.Button,[3] X.D.Cai,[17] M.Campanelli,[51] M.Capell,[17] G.Cara Romeo,[10]
G.Carlino,[31] A.M.Cartacci,[18] J.Casaus,[28] G.Castellini,[18] F.Cavallari,[39] N.Cavallo,[31] C.Cecchi,[21] M.Cerrada,[28]
F.Cesaroni,[25] M.Chamizo,[28] Y.H.Chang,[53] U.K.Chaturvedi,[20] S.V.Chekanov,[33] M.Chemarin,[27] A.Chen,[53] G.Chen,[8]
G.M.Chen,[8] H.F.Chen,[22] H.S.Chen,[8] X.Chereau,[4] G.Chiefari,[31] C.Y.Chien,[5] L.Cifarelli,[41] F.Cindolo,[10] C.Civinini,[18]
I.Clare,[17] R.Clare,[17] H.O.Cohn,[34] G.Coignet,[4] A.P.Colijn,[2] N.Colino,[28] V.Commichau,[1] S.Costantini,[9] F.Cotorobai,[14]
B.de la Cruz,[28] A.Csilling,[15] T.S.Dai,[17] R.D'Alessandro,[18] R.de Asmundis,[31] A.Degré,[4] K.Deiters,[49] D.della Volpe,[31]
P.Denes,[38] F.DeNotaristefani,[39] D.DiBitonto,[46] M.Diemoz,[39] D.van Dierendonck,[2] F.Di Lodovico,[51] C.Dionisi,[39]
M.Dittmar,[51] A.Dominguez,[42] A.Doria,[31] M.T.Dova,[20,♯] D.Duchesneau,[4] P.Duinker,[2] I.Duran,[43] S.Dutta,[11] S.Easo,[36]
Yu.Efremenko,[34] H.El Mamouni,[27] A.Engler,[37] F.J.Eppling,[17] F.C.Erné,[2] J.P.Ernenwein,[27] P.Extermann,[21] M.Fabre,[49]
R.Faccini,[39] S.Falciano,[39] A.Favara,[18] J.Fay,[27] O.Fedin,[40] M.Felcini,[51] B.Fenyi,[46] T.Ferguson,[37] F.Ferroni,[39]
H.Fesefeldt,[1] E.Fiandrini,[36] J.H.Field,[21] F.Filthaut,[37] P.H.Fisher,[17] I.Fisk,[42] G.Forconi,[17] L.Fredj,[21] K.Freudenreich,[51]
C.Furetta,[29] Yu.Galaktionov,[30,17] S.N.Ganguli,[11] P.Garcia-Abia,[50] S.S.Gau,[13] S.Gentile,[39] N.Gheordanescu,[14]
S.Giagu,[39] S.Goldfarb,[24] J.Goldstein,[12] Z.F.Gong,[22] A.Gougas,[5] G.Gratta,[35] M.W.Gruenewald,[9] V.K.Gupta,[38]
A.Gurtu,[11] L.J.Gutay,[48] B.Hartmann,[1] A.Hasan,[32] D.Hatzifotiadou,[10] T.Hebbeker,[9] A.Hervé,[19] W.C.van Hoek,[33]
H.Hofer,[51] S.J.Hong,[45] H.Hoorani,[37] S.R.Hou,[53] G.Hu,[5] V.Innocente,[19] K.Jenkes,[1] B.N.Jin,[8] L.W.Jones,[3] P.de Jong,[19]
I.Josa-Mutuberria,[28] A.Kasser,[24] R.A.Khan,[20] D.Kamrad,[50] Yu.Kamyshkov,[34] J.S.Kapustinsky,[26] Y.Karyotakis,[4]
M.Kaur,[20,◇] M.N.Kienzle-Focacci,[21] D.Kim,[39] D.H.Kim,[45] J.K.Kim,[45] S.C.Kim,[45] Y.G.Kim,[45] W.W.Kinnison,[26]
A.Kirkby,[35] D.Kirkby,[35] J.Kirkby,[19] D.Kiss,[15] W.Kittel,[33] A.Klimentov,[17,30] A.C.König,[33] A.Kopp,[50] I.Korolko,[30]
V.Koutsenko,[17,30] R.W.Kraemer,[37] W.Krenz,[1] A.Kunin,[17,30] P.Ladron de Guevara,[28] I.Laktineh,[27] G.Landi,[18]
C.Lapoint,[17] K.Lassila-Perini,[51] P.Laurikainen,[23] M.Lebeau,[19] A.Lebedev,[17] P.Lebrun,[27] P.Lecomte,[51] P.Lecoq,[19]
P.Le Coultre,[51] J.M.Le Goff,[19] R.Leiste,[50] E.Leonardi,[39] P.Levtchenko,[40] C.Li,[22] C.H.Lin,[53] W.T.Lin,[53] F.L.Linde,[2,19]
L.Lista,[31] Z.A.Liu,[8] W.Lohmann,[50] E.Longo,[39] W.Lu,[35] Y.S.Lu,[8] K.Lübelsmeyer,[1] C.Luci,[39] D.Luckey,[17] L.Luminari,[39]
W.Lustermann,[49] W.G.Ma,[22] M.Maity,[11] G.Majumder,[11] L.Malgeri,[39] A.Malinin,[30] C.Maña,[28] D.Mangeol,[33]
S.Mangla,[11] P.Marchesini,[51] A.Marin,[12] J.P.Martin,[27] F.Marzano,[39] G.G.G.Massaro,[2] D.McNally,[19] R.R.McNeil,[7]
S.Mele,[31] L.Merola,[31] M.Meschini,[18] W.J.Metzger,[33] M.von der Mey,[1] Y.Mi,[24] A.Mihul,[14] A.J.W.van Mil,[33]
G.Mirabelli,[39] J.Mnich,[19] P.Molnar,[9] B.Monteleoni,[18] R.Moore,[3] S.Morganti,[39] T.Moulik,[11] R.Mount,[35] S.Müller,[1]
F.Muheim,[21] A.J.M.Muijs,[2] S.Nahn,[17] M.Napolitano,[31] F.Nessi-Tedaldi,[51] H.Newman,[35] T.Niessen,[1] A.Nippe,[1]
A.Nisati,[39] H.Nowak,[50] Y.D.Oh,[45] H.Opitz,[1] G.Organtini,[39] R.Ostonen,[23] C.Palomares,[28] D.Pandoulas,[1] S.Paoletti,[39]
P.Paolucci,[31] H.K.Park,[37] I.H.Park,[45] G.Pascale,[39] G.Passaleva,[18] S.Patricelli,[31] T.Paul,[13] M.Pauluzzi,[36] C.Paus,[1]
F.Pauss,[51] D.Peach,[19] Y.J.Pei,[1] S.Pensotti,[29] D.Perret-Gallix,[4] B.Petersen,[33] S.Petrak,[9] A.Pevsner,[5] D.Piccolo,[31]
M.Pieri,[18] J.C.Pinto,[37] P.A.Piroué,[38] E.Pistolesi,[29] V.Plyaskin,[30] M.Pohl,[51] V.Pojidaev,[30,18] H.Postema,[17] N.Produit,[21]
D.Prokofiev,[40] G.Rahal-Callot,[51] N.Raja,[11] P.G.Rancoita,[29] M.Rattaggi,[29] G.Raven,[42] P.Razis,[32]K.Read,[34] D.Ren,[51]
M.Rescigno,[39] S.Reucroft,[13] T.van Rhee,[47] S.Riemann,[50] K.Riles,[3] A.Robohm,[51] J.Rodin,[17] B.P.Roe,[3] L.Romero,[28]
S.Rosier-Lees,[4] Ph.Rosselet,[24] W.van Rossum,[47] S.Roth,[1] J.A.Rubio,[19] D.Ruschmeier,[9] H.Rykaczewski,[51] J.Salicio,[19]
E.Sanchez,[28] M.P.Sanders,[33] M.E.Sarakinos,[23] S.Sarkar,[11] M.Sassowsky,[1] C.Schäfer,[1] V.Schegelsky,[40]
S.Schmidt-Kaerst,[1] D.Schmitz,[1] P.Schmitz,[1] N.Scholz,[51] H.Schopper,[52] D.J.Schotanus,[33] J.Schwenke,[1] G.Schwering,[1]
C.Sciacca,[31] D.Sciarrino,[21] L.Servoli,[36] S.Shevchenko,[35] N.Shivarov,[44] V.Shoutko,[30] J.Shukla,[26] E.Shumilov,[30]
A.Shvorob,[35] T.Siedenburg,[1] D.Son,[45] A.Sopczak,[50] B.Smith,[17] P.Spillantini,[18] M.Steuer,[17] D.P.Stickland,[38] A.Stone,[7]
H.Stone,[38] B.Stoyanov,[44] A.Straessner,[1] K.Strauch,[16] K.Sudhakar,[11] G.Sultanov,[20] L.Z.Sun,[22] G.F.Susinno,[21]
H.Suter,[51] J.D.Swain,[20] X.W.Tang,[8] L.Tauscher,[6] L.Taylor,[13] Samuel C.C.Ting,[17] S.M.Ting,[17] M.Tonutti,[1]
S.C.Tonwar,[11] J.Tóth,[15] C.Tully,[38] H.Tuchscherer,[46] K.L.Tung,[8]Y.Uchida,[17] J.Ulbricht,[51] U.Uwer,[19] E.Valente,[39]
R.T.Van de Walle,[33] G.Vesztergombi,[15] I.Vetlitsky,[30] G.Viertel,[51] M.Vivargent,[4] R.Völkert,[50] H.Vogel,[37] H.Vogt,[50]
I.Vorobiev,[30] A.A.Vorobyov,[40] A.Vorvolakos,[32] M.Wadhwa,[6] W.Wallraff,[1] J.C.Wang,[17] X.L.Wang,[22] Z.M.Wang,[22]
A.Weber,[1] F.Wittgenstein,[19] S.X.Wu,[20] S.Wynhoff,[1] J.Xu,[12] Z.Z.Xu,[22] B.Z.Yang,[22] C.G.Yang,[8] X.Y.Yao,[8] J.B.Ye,[22]
S.C.Yeh,[53] J.M.You,[37] An.Zalite,[40] Yu.Zalite,[40] P.Zemp,[51] Y.Zeng,[1] Z.Zhang,[8] Z.P.Zhang,[22] B.Zhou,[12] G.Y.Zhu,[8]
R.Y.Zhu,[35] A.Zichichi,[10,19,20] F.Ziegler.[50]

1 I. Physikalisches Institut, RWTH, D-52056 Aachen, FRG[§]
III. Physikalisches Institut, RWTH, D-52056 Aachen, FRG[§]
2 National Institute for High Energy Physics, NIKHEF, and University of Amsterdam, NL-1009 DB Amsterdam, The Netherlands
3 University of Michigan, Ann Arbor, MI 48109, USA
4 Laboratoire d'Annecy-le-Vieux de Physique des Particules, LAPP,IN2P3-CNRS, BP 110, F-74941 Annecy-le-Vieux CEDEX, France
5 Johns Hopkins University, Baltimore, MD 21218, USA
6 Institute of Physics, University of Basel, CH-4056 Basel, Switzerland
7 Louisiana State University, Baton Rouge, LA 70803, USA
8 Institute of High Energy Physics, IHEP, 100039 Beijing, China[△]
9 Humboldt University, D-10099 Berlin, FRG[§]
10 University of Bologna and INFN-Sezione di Bologna, I-40126 Bologna, Italy
11 Tata Institute of Fundamental Research, Bombay 400 005, India
12 Boston University, Boston, MA 02215, USA
13 Northeastern University, Boston, MA 02115, USA
14 Institute of Atomic Physics and University of Bucharest, R-76900 Bucharest, Romania
15 Central Research Institute for Physics of the Hungarian Academy of Sciences, H-1525 Budapest 114, Hungary[‡]
16 Harvard University, Cambridge, MA 02139, USA
17 Massachusetts Institute of Technology, Cambridge, MA 02139, USA
18 INFN Sezione di Firenze and University of Florence, I-50125 Florence, Italy
19 European Laboratory for Particle Physics, CERN, CH-1211 Geneva 23, Switzerland
20 World Laboratory, FBLJA Project, CH-1211 Geneva 23, Switzerland
21 University of Geneva, CH-1211 Geneva 4, Switzerland
22 Chinese University of Science and Technology, USTC, Hefei, Anhui 230 029, China[△]
23 SEFT, Research Institute for High Energy Physics, P.O. Box 9, SF-00014 Helsinki, Finland
24 University of Lausanne, CH-1015 Lausanne, Switzerland
25 INFN-Sezione di Lecce and Universitá Degli Studi di Lecce, I-73100 Lecce, Italy
26 Los Alamos National Laboratory, Los Alamos, NM 87544, USA
27 Institut de Physique Nucléaire de Lyon, IN2P3-CNRS,Université Claude Bernard, F-69622 Villeurbanne, France
28 Centro de Investigaciones Energeticas, Medioambientales y Tecnologicas, CIEMAT, E-28040 Madrid, Spain♭
29 INFN-Sezione di Milano, I-20133 Milan, Italy
30 Institute of Theoretical and Experimental Physics, ITEP, Moscow, Russia
31 INFN-Sezione di Napoli and University of Naples, I-80125 Naples, Italy
32 Department of Natural Sciences, University of Cyprus, Nicosia, Cyprus
33 University of Nijmegen and NIKHEF, NL-6525 ED Nijmegen, The Netherlands
34 Oak Ridge National Laboratory, Oak Ridge, TN 37831, USA
35 California Institute of Technology, Pasadena, CA 91125, USA
36 INFN-Sezione di Perugia and Universitá Degli Studi di Perugia, I-06100 Perugia, Italy
37 Carnegie Mellon University, Pittsburgh, PA 15213, USA
38 Princeton University, Princeton, NJ 08544, USA
39 INFN-Sezione di Roma and University of Rome, "La Sapienza", I-00185 Rome, Italy
40 Nuclear Physics Institute, St. Petersburg, Russia
41 University and INFN, Salerno, I-84100 Salerno, Italy
42 University of California, San Diego, CA 92093, USA
43 Dept. de Fisica de Particulas Elementales, Univ. de Santiago, E-15706 Santiago de Compostela, Spain
44 Bulgarian Academy of Sciences, Central Lab. of Mechatronics and Instrumentation, BU-1113 Sofia, Bulgaria
45 Center for High Energy Physics, Korea Adv. Inst. of Sciences and Technology, 305-701 Taejon, Republic of Korea
46 University of Alabama, Tuscaloosa, AL 35486, USA
47 Utrecht University and NIKHEF, NL-3584 CB Utrecht, The Netherlands
48 Purdue University, West Lafayette, IN 47907, USA
49 Paul Scherrer Institut, PSI, CH-5232 Villigen, Switzerland
50 DESY-Institut für Hochenergiephysik, D-15738 Zeuthen, FRG
51 Eidgenössische Technische Hochschule, ETH Zürich, CH-8093 Zürich, Switzerland
52 University of Hamburg, D-22761 Hamburg, FRG
53 High Energy Physics Group, Taiwan, China
§ Supported by the German Bundesministerium für Bildung, Wissenschaft, Forschung und Technologie
‡ Supported by the Hungarian OTKA fund under contract numbers T14459 and T24011.
♭ Supported also by the Comisión Interministerial de Ciencia y Technología
♯ Also supported by CONICET and Universidad Nacional de La Plata, CC 67, 1900 La Plata, Argentina
◇ Also supported by Panjab University, Chandigarh-160014, India
△ Supported by the National Natural Science Foundation of China.

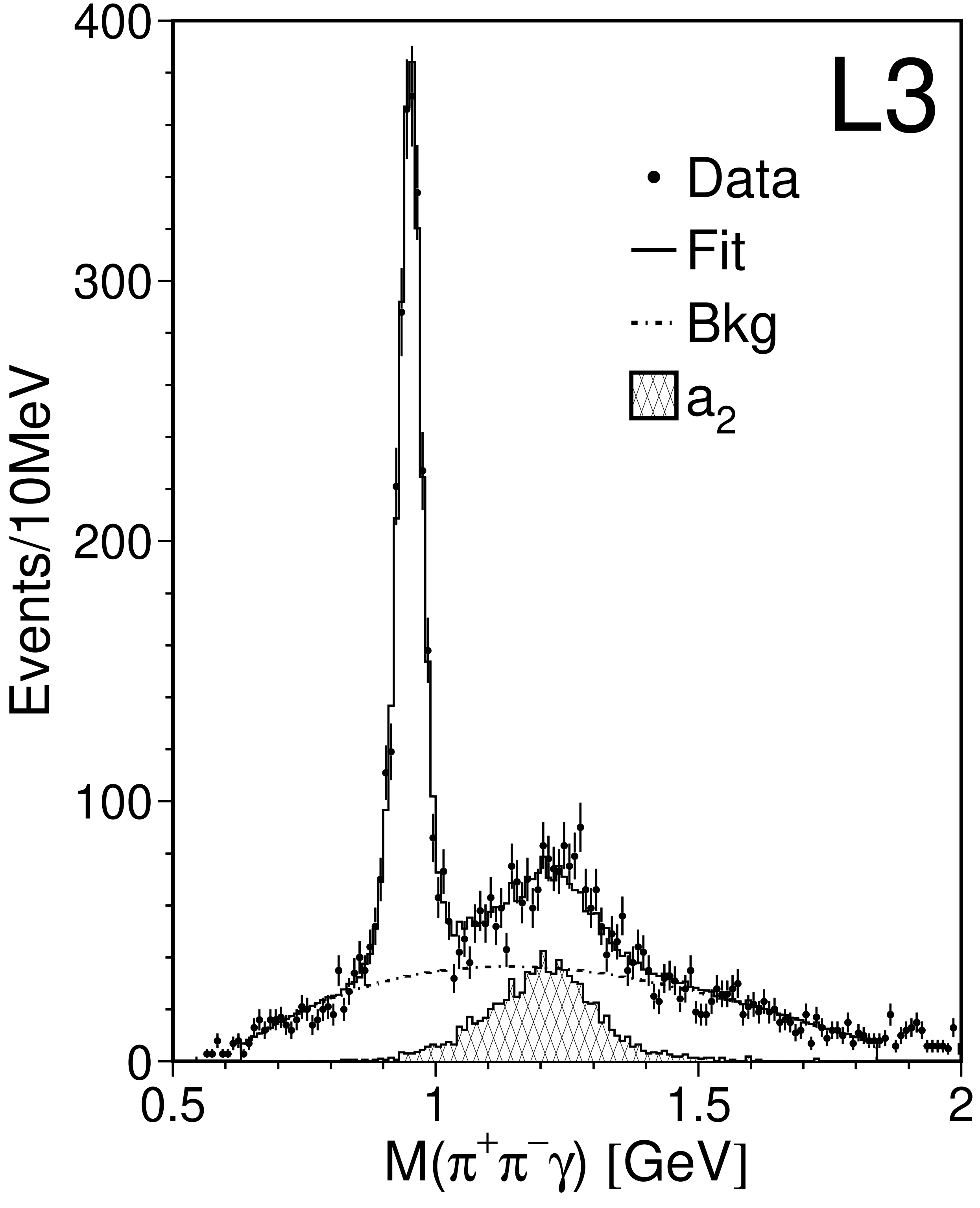

Figure 1: $\pi^+\pi^-\gamma$ reconstructed mass spectrum for the events selected with $Q^2 < 0.01$ GeV^2 . The histogram is the result of the fit described in the text. The shaded area is the a_2 contribution, the dashed-dotted line the third order polynomial background.

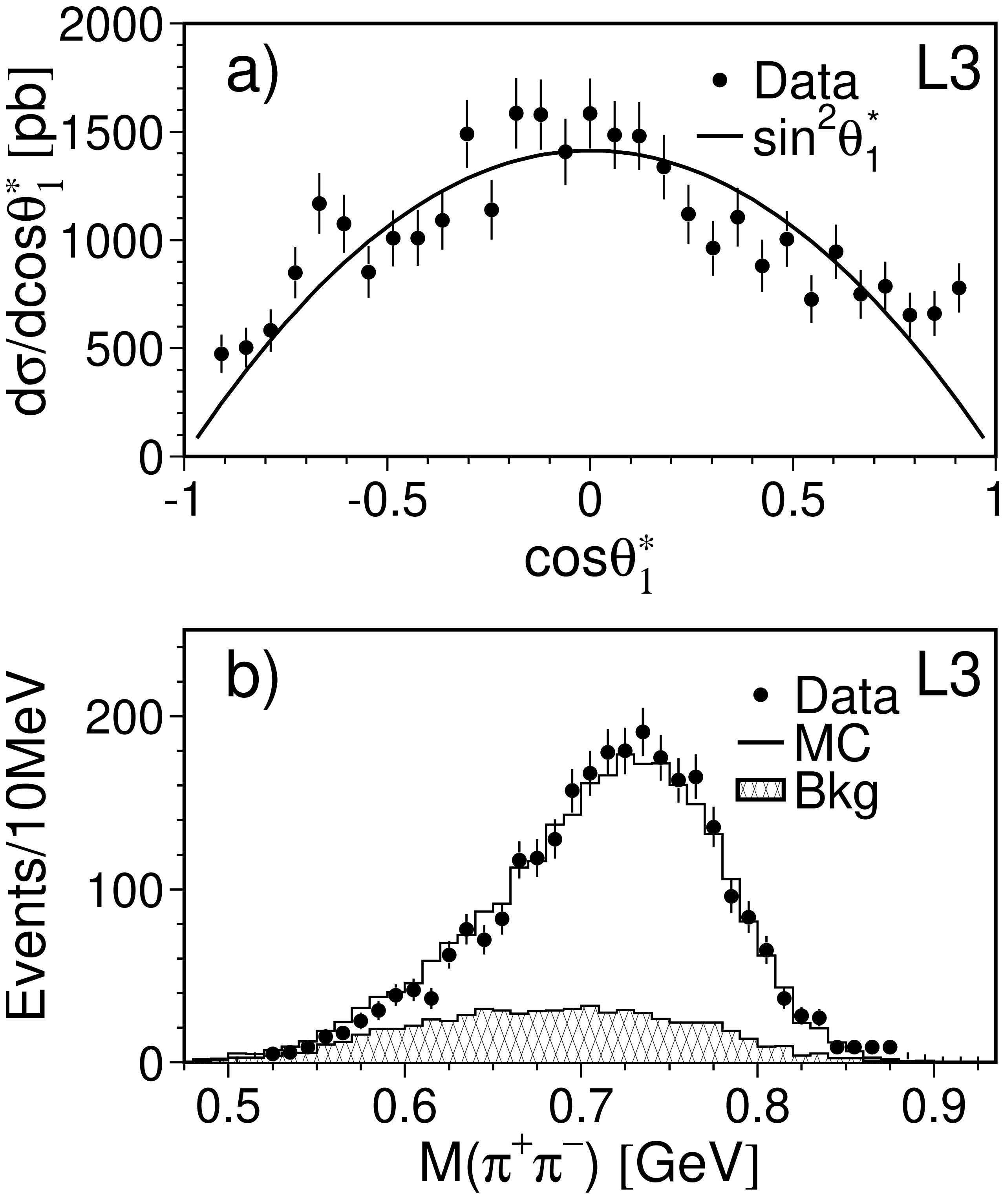

Figure 2: a) Background subtracted and efficiency corrected angular distribution of the π^+ in the ρ helicity frame. The data are fitted to a $\sin^2\theta_1^*$ function. b) The uncorrected $\pi^+\pi^-$ effective mass distribution. The histogram is the prediction of the Monte Carlo which best fits the data ($m_\rho = 766$ MeV and $\Gamma_\rho = 150$ MeV). The shaded area is the background from a_2 and other inclusive processes.

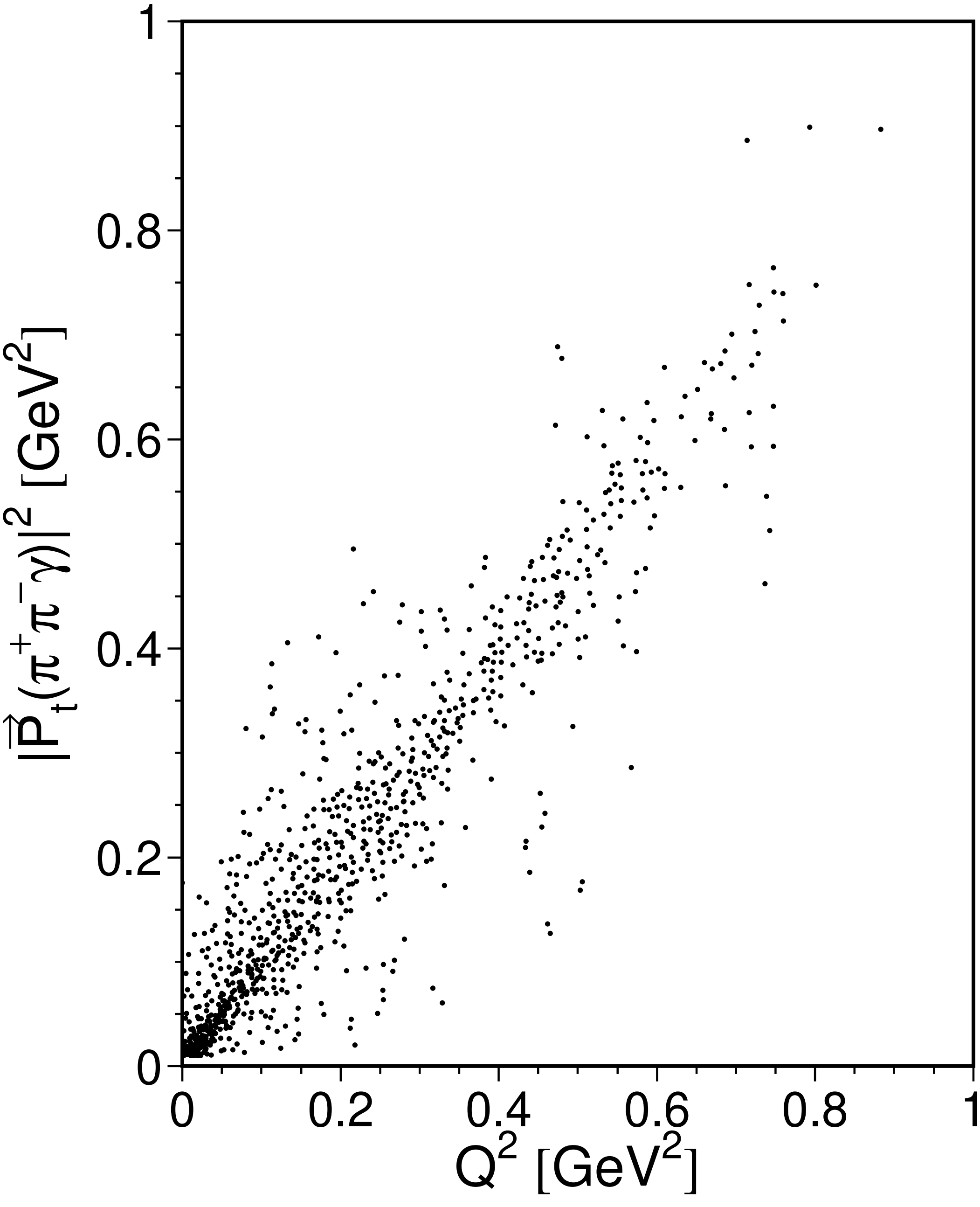

Figure 3: The transverse momentum squared of the reconstructed final state $\pi^+\pi^-\gamma$ versus the generated Q^2.

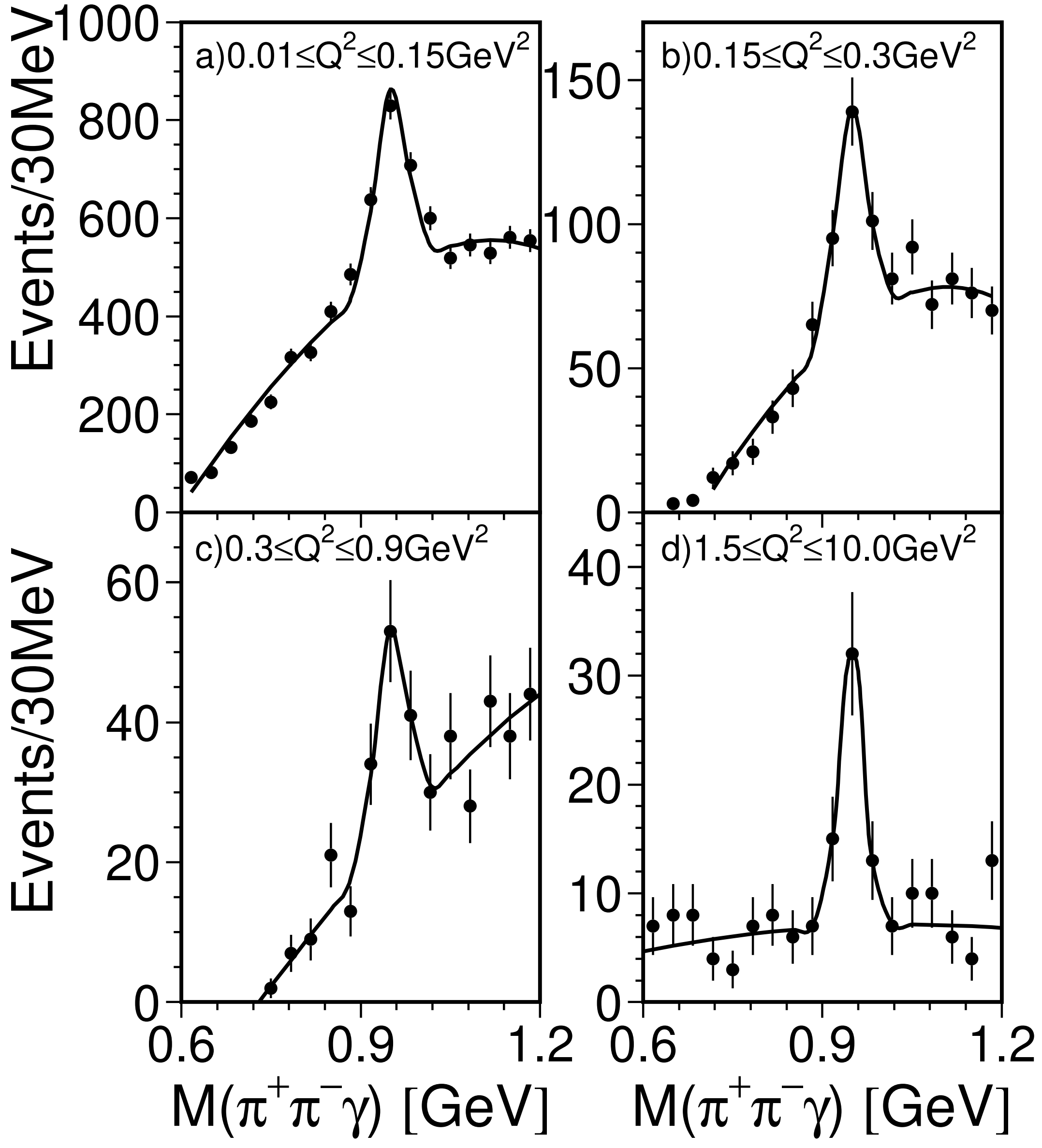

Figure 4: $\pi^+\pi^-\gamma$ mass for the events with high Q^2, separated in four Q^2 intervals: a) $0.01 \leq Q^2 \leq 0.15$ GeV^2, b) $0.15 \leq Q^2 \leq 0.30$ GeV^2, c) $0.30 \leq Q^2 \leq 0.90$ GeV^2, d) Tagged events, $1.5 \leq Q^2 \leq 10.0$ GeV^2.

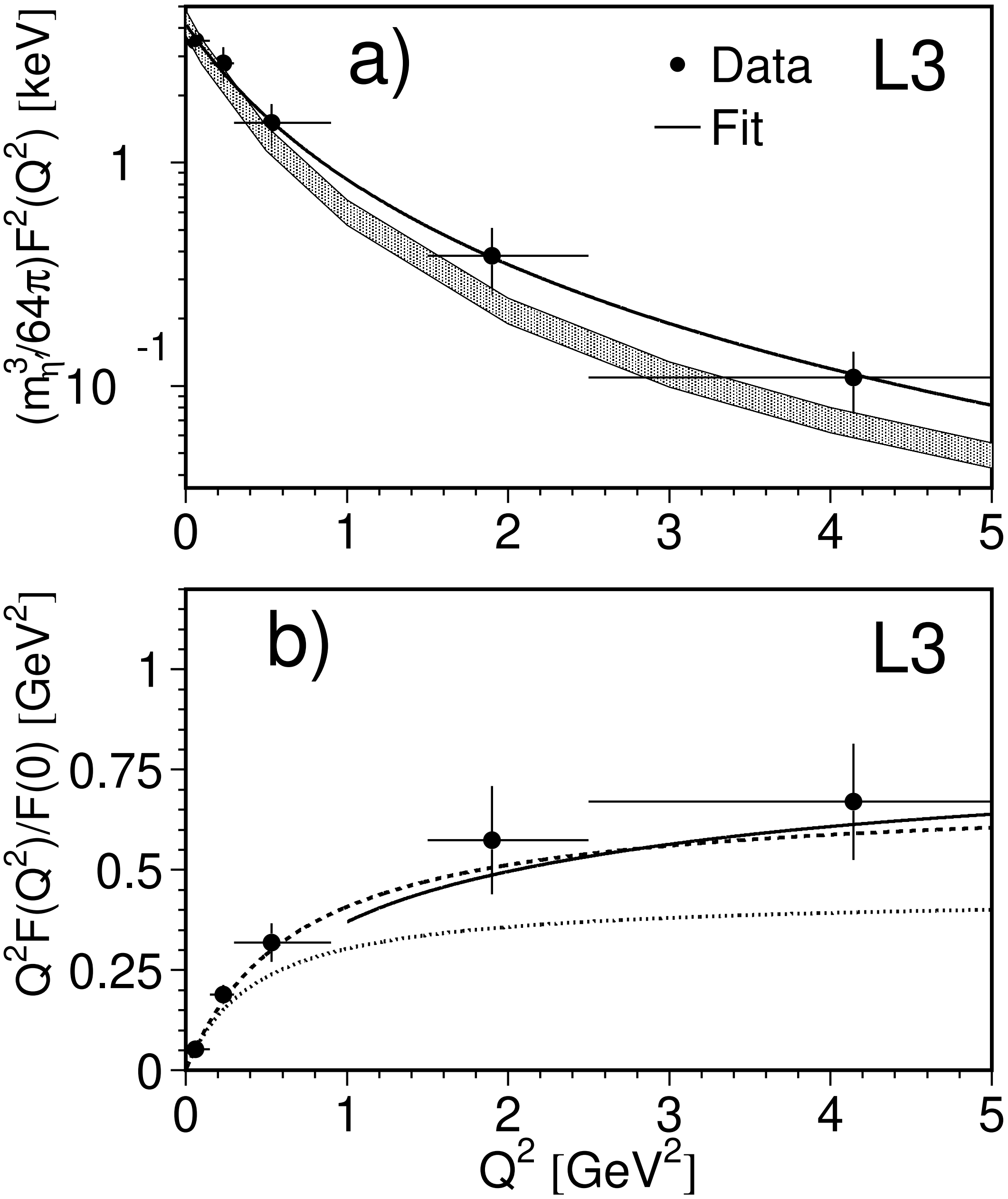

Figure 5: a) $F^2(Q^2)$ as measured at $\sqrt{s}$= 91 GeV. Statistical and systematic errors are added in quadrature. The solid line is the result of the pole fit to the data points described in the text. The predictions of Ref. [19] are indicated as a shaded area, ranging from no gluonium content (upper line) to 15 % of gluonium content (lower line). b) The same date are given as $Q^2F(Q^2)$, normalised to $F(Q^2 = 0)$. The data are compared to QCD calculations [17] (continous line), to VMD predictions [1] (dashed line) and to Ref. [13] (dotted) line.